Performance Modeling of the Ballard Mark IV Solid Polymer Electrolyte Fuel Cell

II. Empirical Model Development

J. C. Amphlett, R. M. Baumert, R. F. Mann, B. A. Peppley, and P. R. Roberge*

Royal Military College of Canada, Kingston, Ontario, Canada K7K 5L0

T. J. Harris

Queen's University, Kingston, Ontario, Canada

ABSTRACT

A parametric model predicting the performance of a solid polymer electrolyte, proton exchange membrane (PEM) fuel cell has been developed using a combination of mechanistic and empirical modeling techniques. This paper details the empirical analysis which yielded the parametric coefficients employed in the model. A 28 run experiment covering a range of operating currents (50 to 300 ASF), temperatures (328 to 358 K), oxygen partial pressures (0.6 to 3.1 atm abs.) and hydrogen partial pressures (2.0 to 3.1 atm abs.) was conducted. Parametric equations for the activation overvoltage and the internal resistance of the fuel cell were obtained from linear regression. The factors to be employed in the linear regression had been previously determined through a mechanistic analysis of fuel cell processes. Activation overvoltage was modeled as a function of the operating temperature, the product of operating temperature, and the logarithm of the operating current, and the product of operating temperature and the logarithm of the oxygen concentration at the catalyst reaction sites. The internal resistance of the fuel cell was modeled as a function of the operating temperature and the current. Correlation of the empirical model to experimental data was very good. It is anticipated that the mechanistic validity yielded by the coupling of mechanistic and empirical modeling techniques will also allow for accurate predictive capabilities outside of the experimental range.

A mechanistic model defining the factors most likely to influence fuel cell performance has been described previously.[1,2] The performance of a fuel cell (output voltage) was defined as a function of the thermodynamic potential, the activation overvoltage, and the ohmic overvoltage, with mass transport losses being incorporated in each of the three terms

$$V = E + \eta_{act} + \eta_{ohmic} \quad [1]$$

The thermodynamic potential E was defined via a Nernst equation as

$$E = 1.229 - 0.85 \cdot 10^{-3}(T - 298.15) + 4.3085 \cdot 10^{-5} \cdot T \cdot \left[\ln(p^*_{H_2}) + \frac{1}{2}\ln(p^*_{O_2})\right] \quad [2]$$

The activation overvoltage was defined as

$$\eta_{act} = \frac{(-\Delta F_e)}{\alpha_c nF} + \frac{(-\Delta F_{ec})}{2F} + \left[\frac{R}{\alpha_c nF}\ln(nFAk^0)(c_{H^+})^{(1-\alpha_c)}(c_{H_2O})^{\alpha_c} + \frac{R}{2F}\ln(4FAk^0)\right]\cdot[T] + \left[\frac{R(1-\alpha_c)}{\alpha_c nF}\right]\cdot[T\ln(c^*_{O_2})] + \left[\frac{R}{2F}\right]\cdot[T\ln(c^*_{H_2})] - \left[\frac{R}{\alpha_c nF} - \frac{R}{2F}\right]\cdot[T\ln(i)] \quad [3]$$

which was rendered to parametric form as

$$\eta_{act} = \xi_1 + \xi_2 T + \xi_3 T[\ln(c^*_{O_2})] + \xi_4 T[\ln(i)] \quad [4]$$

where the ξs represent constant parametric coefficients that are evaluated from experimental data. Fuel composition changes (changes in the hydrogen concentration via dilution with CO_2) were expected to have a negligible effect on fuel cell kinetics over the experimental range (*i.e.*, hydrogen mole fractions >60%) and were not included in the activation model.

Finally, the internal resistance was defined simply to be an unknown function of current and temperature, where the ohmic overvoltage was defined by an Ohm's law expression

$$\eta_{ohmic} = -(i \cdot R^{internal}) \quad [5]$$

Equations 2 through 5 fully define the output voltage of the fuel cell, assuming that flooding or dehydration effects in the fuel cell membrane and electrodes are negligible.

Experimental

Goal of the experimental study.—The goal of the experimental study was to generate sufficient data to:

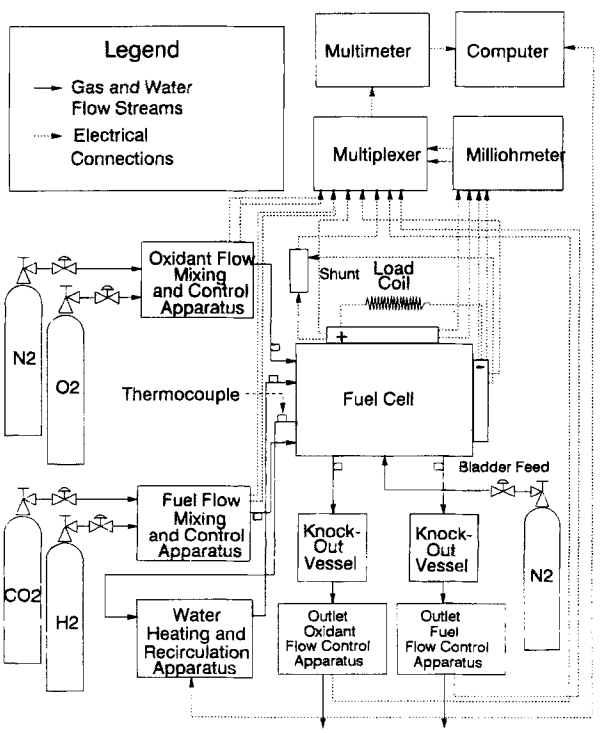

Fig. 1. Schematic diagram of the experimenal apparatus.

* Electrochemical Society Active Member.

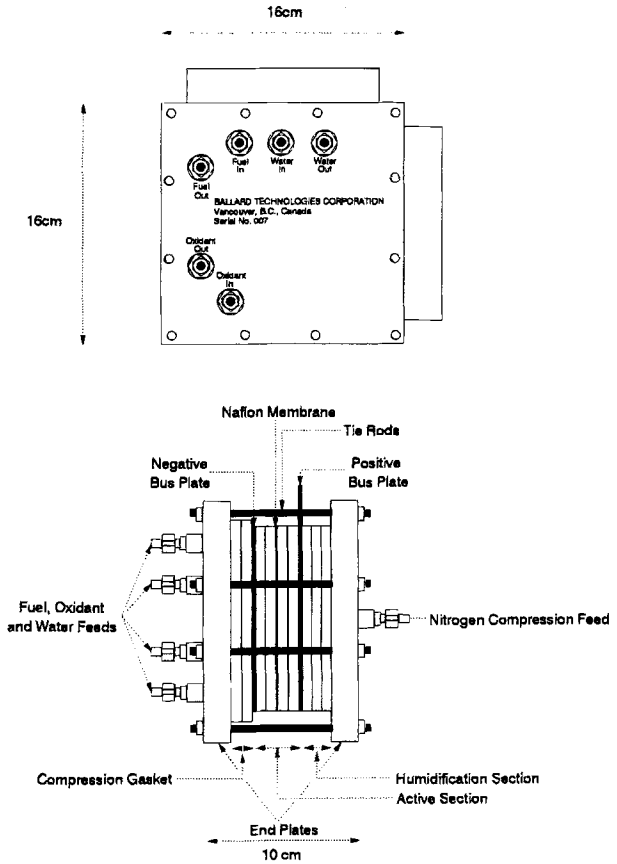

Fig. 2. Ballard Mark IV single fuel cell (R.M.C. cell No. 6).

1. Calculate the thermodynamic equilibrium potential for each run via Eq. 2.
2. Develop an empirical model for activation overvoltage based on the variables proposed in Eq. 3.
3. Develop an empirical model for the internal resistance of the fuel cell as a function of current and temperature.
4. Statistically evaluate the resulting parametric models.

Experimental apparatus.—A schematic diagram of the apparatus employed in this experiment is shown in Fig. 1.

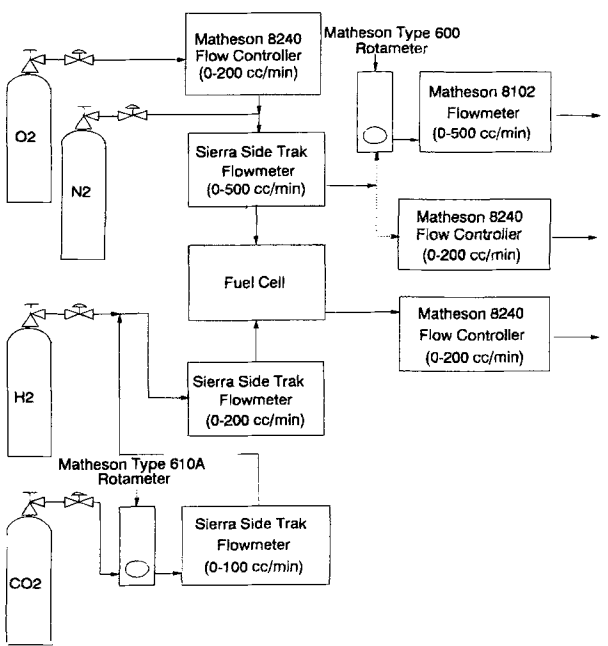

Fig. 3. Pressure-regulated gas flow mixing system.

Table I. Variable settings for experimental design.

Setting	Temperature (K)	Current (A)	p_{O2}^{inlet} (atm)	p_{H2}^{inlet} (atm)
Low	328	2.72	0.6	2.0
Medium	343	6.66	1.4	2.5
High	358	16.33	3.1	3.1

The fuel cell employed for the experiment was a Ballard Mark IV single cell (R.M.C. cell no. 6) as shown in Fig. 2. The Mark IV employs a Nafion membrane (0.18 mm in thickness), with an active surface area of 50.56 cm^2, heat-bonded to two catalyst-coated carbon fiber-paper electrodes. This membrane electrode assembly (MEA) is sandwiched between two graphite current collector plates. The resulting cell is then connected to a humidifying section, compressed pneumatically, and finally sandwiched between two stainless steel end caps.

The gases employed in this experiment were Linde Extra-Dry grade compressed gases (CO_2 is Bone-Dry grade). During the experiment, a pressure-regulated gas flow mixing system, as shown in Fig. 3, was employed. Calibration via a soap film meter indicated that all of the flowmeters and controllers operated within ±2% of full scale. The pressure for all of the inlet gas streams was regulated via Matheson pressure regulators on the gas cylinders.

The current of the fuel cell system was monitored across a 50 A, 50 MV shunt with a Fluke 8840 multimeter. Currents were adjusted by moving contact clips on a copper resistance coil to adjust the resistance of the external load. Using this method, the current could be maintained within ±0.02 A of the desired setting. Fuel cell voltage was monitored across the bus plates with a Fluke 8840 multimeter. The combined resistance of the fuel cell in parallel with the external load was measured via a Hewlett Packard 4328A milliohmeter connected across the bus plates. A mathematical calculation was used to derive the internal resistance from this combined value.

Fuel cell temperature was measured via an ice-water-referenced J-type thermocouple probe, mounted in the exhaust humidification water stream, and monitored through a Fluke 8840 multimeter. The humidification water temperature was controlled via a heating sock, activated by a computer controlled on/off relay switch.

Data acquisition and analysis were provided by a Hewlett Packard Type 86B PC linked via a Data I/O bus to the Fluke 8840 multimeters.

Experimental Design

With the experimental apparatus configured to monitor all of the necessary variables, a three-level experimental design using 28 runs was employed to generate the data required for the linear regression analysis. The independent variables (factors) controlled in the experiment were the fuel cell temperature, the operating current, and the inlet partial pressures of hydrogen and oxygen (total dry gas pressure was kept constant). The dependent variables monitored included the output voltage (V) and the total resistance (internal and load resistance in parallel). Given the acquired data, separation of the monitored resistance into internal and load components allowed for determination of the actual ohmic overvoltage via Eq. 5. Equation 2 allowed for the calculation of the E value. Finally the activation overvoltage was determined via Eq. 1.

The various factor settings are shown in Table I. The temperature range chosen (328 to 358 K) is fairly standard for operation of PEM fuel cells. Operation at lower temperatures is possible but is not considered worthwhile as the output voltage is substantially reduced. The partial pressure settings were achieved by maintaining the total dry gas pressure at both the anode and the cathode constant at 3.06 atm abs. (45 psia, a fairly standard setting for the Mark IV cell[3,4]), and varying the oxygen and hydrogen mole fractions in the dry oxidant and fuel feeds. Dry-basis mole fraction settings were 0.21, 0.46, and 1.00 for oxygen, and

0.65, 0.81, and 1.00 for hydrogen. In this way the full range of probable oxidant and fuel feeds was covered, from air to pure oxygen and from a simulated reformed hydrocarbon to pure hydrogen.

The experimental current range was limited by the maximum control capacity of the oxidant flow-mixing apparatus (250 cm^3/min) which restricted the experimental range to currents less than 17 A (although verification of the model at currents outside of the experimental range could be achieved using pure oxygen or premixed air feeds). The fuel cell itself was limited to currents of less than 28 A due to resistances within the wires connecting the shunt and the bus plates.

The choice of which variables to control in the experiment was made early in the development process of the model, before many of the insights provided by mechanistic modeling were incorporated. At the time the experiment was conducted, it was considered that a linear regression of output voltage onto the various effects of the variables T, ln (i), ln ($p_{O_2}^{inlet}$), and ln ($p_{H_2}^{inlet}$), could yield a sufficiently accurate model. This assumption was based, in part, upon previous empirical modeling efforts found in the literature.[5-7] As mechanistic analysis proceeded, however, it became apparent that the independent variables directly involved in the mechanisms of fuel cell operation were different from those controlled in the experiment. However, while the experimental design carried out did not exactly reflect the final models chosen, the information generated was still sufficient to model the desired relationships. In order to reflect the activation overvoltage model suggested by Eq. 4, a three-factor regression model using temperature, the product of temperature and the logarithm of current, and the product of temperature and the logarithm of the effective concentration of oxygen should be used. As the surface concentration can be calculated from the inlet partial pressure, all of these factors could be determined from the original experimental data.

During all runs, stoichiometries of the inlet flows were kept constant at 8.33 cm^3 (STP) of oxidant (cathode gas) per cm^3 of oxygen consumed and 1.73 cm^3 (STP) of fuel (anode gas) for each cm^3 of hydrogen consumed. Previous experimental data had indicated that this ratio of inlet flow to consumption would provide for stable operation in a MkIV cell.[3,4] While the effect of changing flow rates is not assessed directly in the model, it is indirectly monitored in terms of its effect on partial pressures. The main effect of a flow rate change would be a shift in the stoichiometry in terms of inlet cm^3 of oxidant or fuel per cm^3 of oxidant or fuel consumed. As a result, the outlet composition of the fuel and oxidant feeds would change, altering the effective reactant composition at the catalyst sites. Thus the effect of the flow rates is incorporated in the model via the reactant concentration terms. Other effects of changing flow rates, such as flooding of the fuel cell if flow rates are too low to adequately remove product water, are not considered in this model.

Experimental Method

Each experimental run was begun with the fuel cell at room temperature and open circuit (*i.e.*, zero current), with a flow of 300 cm^3/min (STP) of humidified oxygen on the cathode side and 50 cm^3/min (STP) of humidified hydrogen on the anode side. The humidification and heating water was heated to slowly bring the fuel cell to 328 K (55°C). This initialization took between 20 and 25 min to complete. When a temperature of 328 K was achieved, the inlet fuel and oxidant feeds were set to their desired compositions and flow settings, and the operating temperature was brought to the desired level. When the operating temperature was achieved, the external load was connected and adjusted for achieving the desired current. The fuel cell was then allowed to run in this condition, with required adjustment of the load to maintain a stable current setting, until such time as the range in the output voltage over a span of 10 min was observed to be less than 1 mV (the output voltages range from 662 to 910 mV). This definition of steady state was achieved within 60 to 120 min of the application of the load. The output voltage reading and corresponding internal resistance at the end of the 10 min period were recorded. After each run, the external load was disconnected, and the flows were returned to the 300 cm^3/min oxygen and 50 cm^3/min hydrogen condition. The fuel cell was then allowed to cool at open circuit to 308 K (35°C), at which point the flows were stopped entirely, and the fuel cell was allowed to return to room temperature.

Experimental Results and Discussion

Determination of the thermodynamic potential and the overvoltages.—The variable settings used in the 28 experimental runs, along with measured and calculated results, are shown in Table II. The first component of the model to be determined in the analysis of the experimental data is the thermodynamic equilibrium potential, calculated via Eq. 2. Before making this calculation, the effective surface partial pressures p_i^* must be determined. The mathematics employed in this determination are detailed elsewhere.[1,2] Results are shown in Table III. There is little variation in the equilibrium potential between runs, with an overall range of less than 0.03 V.

With the voltage, current, internal resistance, and thermodynamic equilibrium potential known, the experimental values of the ohmic and activation overvoltages can be calculated via Eq. 4, 5, and 1. These values are also shown in Table III. Activation losses, ranging from 0.272 to 0.445 V, are significantly larger than resistance-related losses, which range from 0.105 to 0.011 V over the experimental range studied. Observation of the data shows, however, that the slope of the ohmic overvoltage response is steeper than that of the activation overvoltage, such that the ohmic overvoltage plays an increasingly significant role as currents rise.

Development and evaluation of the activation overvoltage model.—The dependent and independent variables involved in determining the empirical model for activation overvoltage are the temperature, the current, and the effective concentration of oxygen at the cathode catalyst sites, $c_{O_2}^*$. Means for calculation of the latter value are discussed elsewhere,[1,2] and the resulting values are included in Table IV. The parametric expression resulting from a linear

Table II. Experimental settings and results.

Experimental Settings					Measured Results		Calculated Results	
Term	T	i	$p_{O_2}^{in}$	$p_{H_2}^{in}$	V	R^{tot}	R^{ext}	R^{int}
Unit	K	amps	atm abs	atm abs	volts	mΩ	Ω	mΩ
Error (+/-)	0.5	0.02	0.1	0.5	0.0005	0.005	0.003	0.07
Run No.								
1	358	2.72	1.4	2.5	0.910	3.88	0.335	3.93
2	328	6.66	0.6	2.5	0.773	4.89	0.116	5.10
3	343	6.66	1.4	2.5	0.820	4.55	0.123	4.73
4	358	6.66	3.1	2.5	0.867	4.10	0.130	4.23
5	343	6.66	3.1	3.1	0.851	4.53	0.128	4.70
6	343	6.66	0.6	2.0	0.781	4.55	0.117	4.73
7	328	6.66	1.4	2.0	0.802	4.89	0.120	5.10
8	343	2.72	0.6	2.5	0.863	4.20	0.317	4.26
9	343	6.66	1.4	2.5	0.824	4.46	0.124	4.63
10	343	6.66	1.4	2.5	0.827	4.41	0.124	4.57
11	328	2.72	1.4	2.5	0.888	4.95	0.326	5.03
12	328	6.66	3.1	2.5	0.835	5.05	0.125	5.26
13	343	6.66	1.4	2.5	0.826	4.37	0.124	4.53
14	358	6.66	0.6	2.5	0.809	4.06	0.121	4.20
15	358	6.66	1.4	3.1	0.846	3.93	0.127	4.06
16	358	6.66	1.4	2.0	0.836	3.99	0.125	4.12
17	343	16.33	1.4	3.1	0.715	4.77	0.044	5.35
18	343	16.33	3.1	2.5	0.730	4.93	0.045	5.54
19	343	6.66	1.4	2.5	0.823	4.56	0.124	4.74
20	343	6.66	0.6	3.1	0.792	4.41	0.119	4.58
21	358	16.33	1.4	2.5	0.729	4.42	0.045	4.90
22	343	2.72	1.4	3.1	0.901	4.28	0.331	4.34
23	343	6.66	3.1	2.0	0.847	4.44	0.127	4.60
24	343	2.72	1.4	2.0	0.898	4.28	0.330	4.34
25	343	16.33	0.6	2.5	0.662	4.77	0.041	5.40
26	343	6.66	1.4	2.5	0.822	4.56	0.123	4.74
27	328	6.66	1.4	3.1	0.807	5.02	0.121	5.24
28	343	16.33	1.4	2.0	0.700	4.90	0.043	5.53

Table III. Surface partial pressures, thermodynamic equilibrium potentials, and calculated overvoltages.

Term	$p_{O_2}^*$	$p_{H_2}^*$	E	η_{ohmic}	η_{act}
Unit	atm abs	atm abs	volts	volts	volts
Error (+/-)	0.1	0.5	0.004	0.0002	0.005
Run No.					
1	1.3	2.3	1.193	-0.0107	-0.2717
2	0.4	2.1	1.208	-0.0340	-0.4017
3	1.3	2.2	1.204	-0.0315	-0.3522
4	3.0	2.3	1.199	-0.0282	-0.3038
5	3.0	3.2	1.216	-0.0313	-0.3341
6	0.4	1.3	1.189	-0.0315	-0.3756
7	1.3	1.3	1.209	-0.0340	-0.3727
8	0.4	2.2	1.196	-0.0116	-0.3220
9	1.3	2.2	1.204	-0.0309	-0.3492
10	1.3	2.2	1.204	-0.0305	-0.3472
11	1.3	2.1	1.216	-0.0137	-0.3141
12	3.0	2.1	1.222	-0.0351	-0.3520
13	1.3	2.2	1.204	-0.0302	-0.3482
14	0.4	2.3	1.184	-0.0280	-0.3473
15	1.3	3.4	1.199	-0.0271	-0.3250
16	1.3	1.4	1.185	-0.0275	-0.3218
17	1.3	3.2	1.209	-0.0874	-0.4075
18	3.0	2.2	1.210	-0.0905	-0.3902
19	1.3	2.2	1.204	-0.0316	-0.3492
20	0.4	3.2	1.202	-0.0305	-0.3788
21	1.3	2.3	1.192	-0.0800	-0.3834
22	1.3	3.2	1.210	-0.0118	-0.2969
23	3.0	1.3	1.203	-0.0307	-0.3249
24	1.3	1.3	1.197	-0.0118	-0.2868
25	0.4	2.2	1.195	-0.0882	-0.4453
26	1.3	2.2	1.204	-0.0316	-0.3502
27	1.3	3.1	1.221	-0.0349	-0.3793
28	1.2	1.3	1.196	-0.0903	-0.4062

Table IV. Effective surface oxygen concentrations and predicted and residual values for activation overvoltage.

Term	$c_{O_2}^*$	Predicted η_{act}	Residual
Unit	mol/cm^3	volts	volts
Run No.			
1	1.0e-06	-0.2647	-0.0070
2	3.8e-07	-0.4014	-0.0003
3	1.1e-06	-0.3500	-0.0023
4	2.4e-06	-0.3025	-0.0012
5	2.5e-06	-0.3283	-0.0059
6	3.6e-07	-0.3775	0.0019
7	1.1e-06	-0.3747	0.0020
8	3.8e-07	-0.3188	-0.0032
9	1.1e-06	-0.3500	0.0008
10	1.1e-06	-0.3500	0.0028
11	1.2e-06	-0.3193	0.0052
12	2.7e-06	-0.3541	0.0021
13	1.1e-06	-0.3500	0.0018
14	3.4e-07	-0.3537	0.0064
15	1.0e-06	-0.3252	0.0002
16	1.0e-06	-0.3252	0.0035
17	1.0e-06	-0.4083	0.0008
18	2.4e-06	-0.3868	-0.0034
19	1.1e-06	-0.3500	0.0008
20	3.6e-07	-0.3775	-0.0013
21	9.9e-07	-0.3860	0.0026
22	1.1e-06	-0.2920	-0.0049
23	2.5e-06	-0.3283	0.0033
24	1.1e-06	-0.2920	0.0053
25	3.2e-07	-0.4379	-0.0074
26	1.1e-06	-0.3500	-0.0002
27	1.1e-06	-0.3747	-0.0046
28	1.0e-06	-0.4083	0.0021

regression of the three factor model onto the activation overvoltage data from Table III is

$$\eta_{act} = -0.9514 + 0.00312T + 7.4 \cdot 10^{-5}T[\ln (c_{O_2}^*)] - 0.000187T[\ln (i)] \quad [6]$$

As intuitively expected, increases in temperature and oxygen concentration, with their positive effect on kinetic reaction rates, will both tend to decrease the activation overvoltage, while an increase in the current will have the opposite effect. The activation overvoltages predicted by Eq. 6 are plotted in Fig. 4 in a parity plot with the experimental data from Table III. These values are tabulated in Table IV, along with the resultant residuals. Scatterplots of the residuals *vs.* the experimental factors showed no significant trends or outliers.

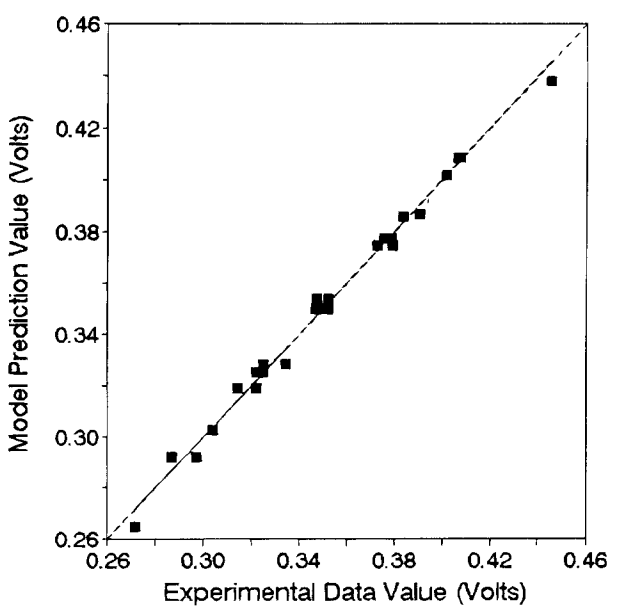

Fig. 4. Parity plot of the model prediction and the experimental data for the fuel cell activation overvoltage.

ANOVA analysis of the model, as shown in Table V, reveals very favorable statistical diagnostics. A very good fit is indicated by the coefficient of determination (R^2) near 1, the very small standard error, and the highly significant F statistic. The standard deviations of the parameter estimates and 95% confidence intervals of the parameters are shown in Table VI. Since none of the confidence intervals enclose zero, all of the parameters are statistically significant.

Given the results of the statistical analysis presented, the model of Eq. 6 is concluded to provide valid and accurate estimates of the overvoltage due to activation over the experimental range observed.

Development and evaluation of the internal resistance model.—Initial mechanistic analysis suggested that the model for the fuel cell's internal resistance should be in some way dependent upon the operating current and the operating temperature.[1,2] As mechanistic modeling did not yield the explicit form which this dependence should take, statistical diagnostics were used to determine which independent variables were correlated to the internal resistance. The two statistical diagnostics used for this purpose were the Pearson's r statistic, and the t statistic. Table VII shows the results of these analyses. The more linear the correlation between a dependent and an independent variable, the closer the absolute value of Pearson's r statistic will be to 1. For the t statistic, the 95% significance value for our analysis was 2.052. Thus the Pearson's r- and t-

Table V. ANOVA table for the activation overvoltage model.

Source of Variance	Degrees of Freedom	Sum of Squares	Mean Square	F	p	R^2	Stand. Error
Regression	3	0.043398	0.014470	943.7	< 0.005	0.992	0.00392
Error	24	0.000368	0.000015				
Lack of fit	18	0.000347	1.9×10^{-5}	5.7	<0.05		
Pure Error	6	0.000020	3.4×10^{-6}				

Table VI. 95% confidence intervals for parameters of the activation overvoltage model.

95 % Confidence Interval				
-0.8951	<	ξ_1	<	-1.0076
0.00331	<	ξ_2	<	0.00292
-0.000178	<	ξ_3	<	-0.000195
8.1×10^{-5}	<	ξ_4	<	6.7×10^{-5}

statistic evaluations indicated that all variables, with the exception of [ln (i)][ln (T)], have a linear relationship with the internal resistance. Thus the independent variables which were concluded to be most colinear with the internal resistance are the main, interaction, and quadratic effects of temperature and current (*i.e.*, T, i, $T(i)$, T^2, and i^2). Linear regression of the five-factor model, however, revealed that the interaction and quadratic effects were negligible and the internal resistance could be modeled linearly on the temperature and the current. The resulting two factor model was

$$R^{\text{internal}} = 0.01605 - 3.5 \cdot 10^{-5}T + 8.0 \cdot 10^{-5}i \qquad [7]$$

As expected, increases in current will increase resistance, while increases in temperature will decrease it. The values predicted by Eq. 7 are shown in Fig. 5 in a parity plot against the experimental data from Table II. Scatterplots of the residuals showed no significant trends or outliers.

Table VIII shows the ANOVA analysis of the internal resistance model. A highly significant F statistic can be observed, as well as a coefficient of determination close to 1, a low standard error, and a highly insignificant lack of fit F statistic. All of these diagnostics indicate a very good fit between the predicted resistance values and the actual data.

The 95% confidence intervals for the parameters are given in Table IX. Since none of the confidence intervals enclose zero, all of the parameters are statistically significant. The results of the statistical analysis presented indicate that Eq. 7 provides accurate estimates of the internal resistance of this fuel cell.

Combined prediction of the output voltage.—Equation 1 indicates that the output voltage of a fuel cell can be stated as a function of the thermodynamic equilibrium potential, the activation overvoltage, and the ohmic overvoltage. Thus Eq. 2, 6, and 7 yield all of the information required to predict the output voltage for a given set of operating conditions. The experimental and predicted output voltages are plotted as a parity plot in Fig. 6. The coefficient of determination (R^2) for the predicted voltage is 0.997, with a standard error of 0.004 V. Scatterplots of the residuals *vs.* actual output voltage and run number reveal no obvious trends or outliers.

Comparisons of the predicted fuel cell voltage and actual fuel cell data can be seen in Fig. 7 through 10. Figure 7 shows the effect of operating current on fuel cell output voltage, for one of the fuel cell operating conditions (oxidant = air, fuel = pure hydrogen, temperature = 343 K, dry gas pressure = 45 psia). The model is shown to accurately correlate fuel cell voltage over the experimental range of current densities and to predict voltages accurately for current densities as high as 470 ASF (170 ASF beyond the experimental range used to evaluate the coefficients), the highest current density achievable with the current fuel cell apparatus. It was observed over the course of the experiment, however, that the open-circuit voltage was significantly lower, at approximately 1.02 to 1.08 V, then the predicted values (1.18 to 1.21 V). An explanation for this discrepancy is that a mixed potential may exist at open circuit, due to the production and decomposition of hydrogen peroxide.[8] As soon as any net current flow exists, the oxygen reduction reaction would take precedence and the thermodynamic equilibrium potential predicted by Eq. 2 would apply. This would explain the very good agreement of predicted and experimental output voltage values at all points other than the open-circuit condition.

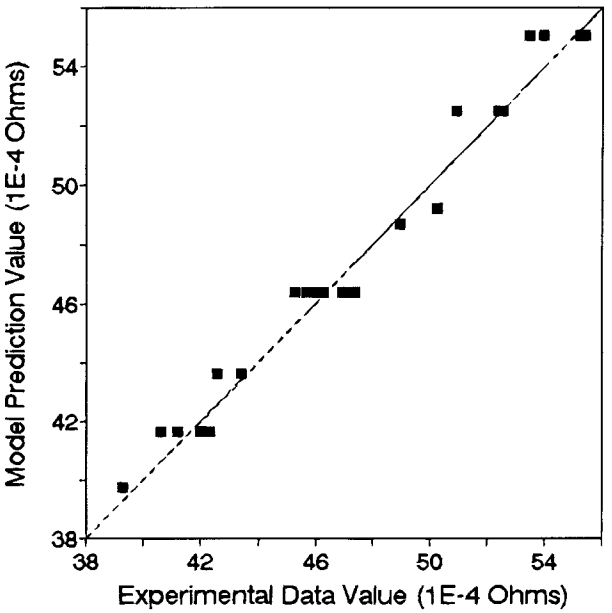

Fig. 5. Parity plot of the model prediction and the experimental data for the fuel cell internal resistance.

Figure 8 shows the effect of temperature on the output voltage of the fuel cell. As the temperature increases, so does the output voltage, rising by approximately 0.002 V/K at a current density of 300 ASF (for the flow compositions indicated). According to the model this increase is attributable to the increase in the rate of reaction, the increased diffusivity of protons and the increased water content in the anode stream at higher temperatures. There is a slight decrease in the thermodynamic equilibrium potential as temperature increases, but this drop is relatively small as compared to the decline in the overvoltages. The good agreement between predicted and experimental values clearly indicates that the model accurately depicts the effect of temperature on output voltage.

Figure 9 shows the effect of changing oxidant composition on the output voltage. As the oxygen concentration in the dry oxidant is increased from 21 to 100%, there is a

Table VII. Correlation diagnostics.

Independent Variable	T	i	Ti	T^2	i^2
Pearson's r-statistic	-0.62	0.72	0.69	-0.64	0.72
t-statistic	4.15	5.55	5.04	4.40	5.48

Independent Variable	ln(T)	ln(i)	[ln(i)][ln(T)]	[T][ln(i)]	[i][ln(T)]
Pearson's r-statistic	-0.40	0.67	0.31	0.61	0.72
t-statistic	2.31	4.82	1.697	4.05	5.46

Table VIII. ANOVA table for the two-factor model of internal resistance.

Source of Variance	Degrees of Freedom	Sum Of Squares	Mean Square	F	p	R^2	Standard Error
Regression	2	5.67e-06	2.84e-06	400.3	< 0.001	0.969	8.4×10^{-5}
Error	25	1.77e-07	7.09e-09				
Lack of Fit	5	3.66e-08	7.31e-09	1.0	>0.25		
Pure Error	20	1.41e-07	7.04e-09				

Table IX. 95% confidence intervals for the parameters of the resistance model.

95 % Confidence Interval				
0.01485	<	γ_1	<	0.01725
-3.8×10^{-5}	<	γ_2	<	-3.1×10^{-5}
7.1×10^{-5}	<	γ_3	<	8.6×10^{-5}

subsequent increase in output voltage of approximately 0.0009 V/%O_2 at a current density of 300 ASF (for the flow compositions indicated). According to the model, this increase is attributable to both thermodynamic and kinetic effects, as an increased oxygen concentration increases the thermodynamic equilibrium potential while decreasing the kinetically controlled activation overvoltage. Once again, good agreement is achieved between model and experimental values, indicating an accurate depiction of the effect of oxidant composition over the experimental range.

Figure 10 shows the effect of changing the fuel composition on the output voltage. As the hydrogen mole fraction in the dry fuel is varied from 65 to 100%, there is a corresponding change in output voltage of 0.0004 V/% H_2 at a current density of 300 ASF (for the flow compositions indicated). This change is not as significant as the change observed for shifts in oxidant composition and is attributed in the model solely to the change in thermodynamic equilibrium potential. The agreement between experimental and model values in this curve is not as good as for the other variables, possibly due to an unmodeled kinetic contribution. Nonetheless, the absolute error between the model and the data is negligible for practical purposes.

A final indication of the success of the modeling exercise is afforded by comparison of the numeric and theoretical values of the parameter coefficients ξ_3 and ξ_4. In the initial mechanistic model,[1,2] these coefficients were defined as

$$\xi_3 = \frac{R}{\alpha_c nF}(1-\alpha_c) \quad [8a]$$

$$\xi_4 = -\left(\frac{R}{\alpha_c nF} + \frac{R}{2F}\right) \quad [8b]$$

while the empirical model gives them the values

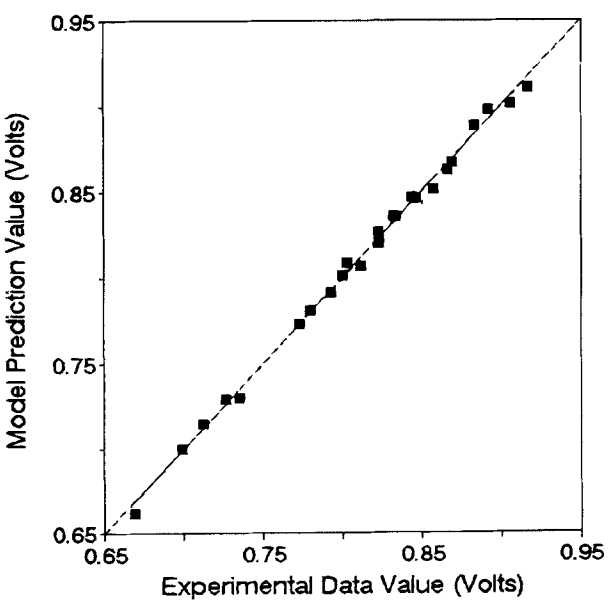

Fig. 6. Parity plot of the model prediction and the experimental data for the total output fuel cell voltage.

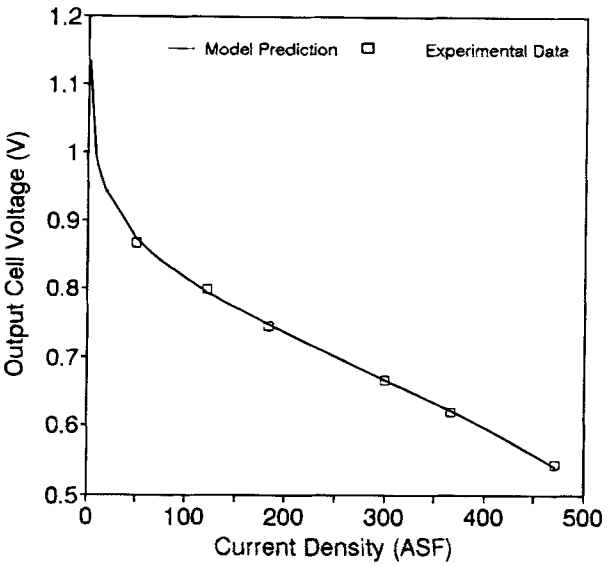

Fig. 7. Effect of operating current on fuel cell output voltage.

$$\xi_3 = 7.4 \cdot 10^{-5} \quad [9a]$$

$$\xi_4 = -0.000187 \quad [9b]$$

The value of n, the number of electrons involved in the rate-determining step of the cathode reaction mechanism, is likely[8] to be 1 or 2. If $n = 2$ is chosen then comparison of the ξ_3 values yields a value for α_c of approximately 0.37, well within the range suggested for the oxygen electrode by Berger (0.2 to 0.45).[5] Substitution of this value of α_c back into Eq. 8b yields a value for ξ_4 of approximately −0.00016, very close to the value actually determined by the empirical analysis. Thus, along with providing good correlation with experimental data, the empirical model is also consistent with mechanistic expectations. The Tafel slope calculated from the empirically determined value of ξ_4, 0.118 at 358 K, is also in agreement with Tafel slope values ($b \sim 0.13$) determined elsewhere for Nafion membranes.[9]

Conclusions

The primary conclusion drawn from this study is that the performance of a solid polymer electrolyte fuel cell can be adequately modeled using a combination of mechanistic and empirical modeling techniques. It is further concluded that the activation overvoltage can be accurately modeled as a function of the temperature and the products [temperature] · [ln (current)] and [temperature] · [ln (effective oxygen concentration)]. It is also concluded that the internal resistance of the fuel cell can be accurately modeled as a function of temperature and current. If the thermodynamic

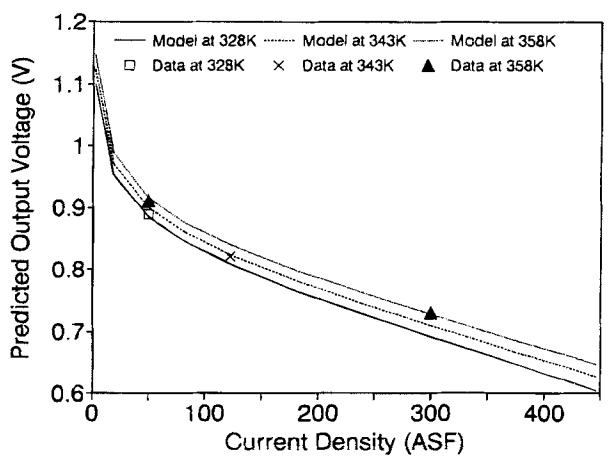

Fig. 8. Effect of temperature on fuel cell output voltage.

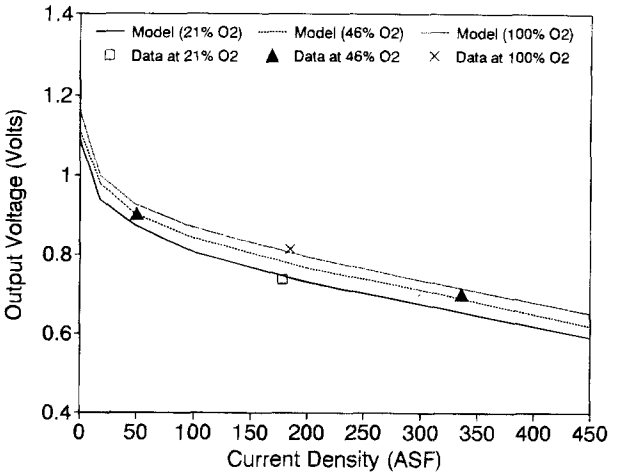

Fig. 9. Effect of changing oxidant composition on output voltage.

equilibrium potential is calculated via the Nernst equation, as defined by Eq. 2, then a combination of the calculated thermodynamic equilibrium potential, the predicted activation overvoltage, and the predicted ohmic overvoltage (taken as the negative of the product of operating current and predicted internal resistance), can be used to accurately predict the output voltage of the fuel cell over a wide range of current densities [$0 < I < 470$ ASF (and possibly higher)], temperatures ($328\ K < T < 358\ K$) and oxidant and fuel compositions (air to pure oxygen, 65% H_2/25% CO_2 to pure hydrogen). Kinetic effects at the cathode are concluded to be highly significant to overall performance, while kinetic effects at the anode appear to be relatively unimportant. Cathode kinetics are concluded to be highly dependent upon the oxidant feed composition, as well as the mass transport and temperature characteristics of the fuel cell.

In summary, the modeling approach used is concluded to be effective, efficient, and easily applied using a small amount of data. It provides a flexible modeling alternative which may be of greater utility than the complex mechanistic models previously proposed,[10-12] due to its greater ease of application.

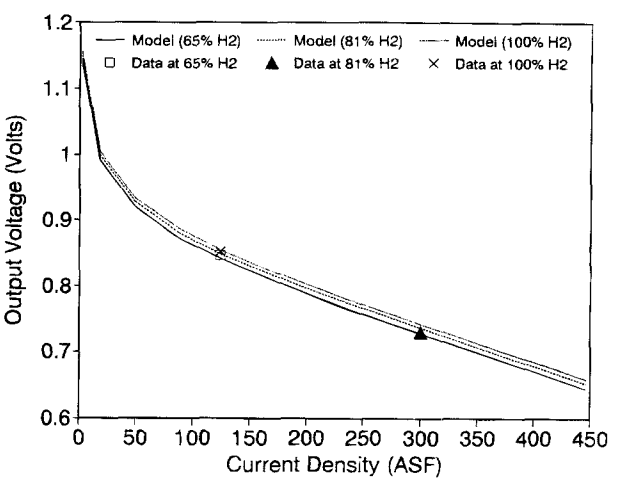

Fig. 10. Effect of changing fuel composition on output voltage.

Manuscript submitted July 1, 1993; revised manuscript received July 25, 1994. This was in part Paper 89 presented at the Toronto, ON, Canada, Meeting of the Society, Oct. 11-16, 1994.

The Royal Military College of Canada assisted in meeting the publication costs of this article.

LIST OF SYMBOLS

c_i	concentration of species i, mol/cm^3
E	thermodynamic equilibrium potential, V
E°	reference potential, V
E_0°	standard state reference potential, V
F	Faraday's constant, 96,487 C/equiv.
I	current density, A/cm^2
i	current, A
i_o	exchange current, A
k°	intrinsic rate constant
n	number of equivalents involved in a reaction
P	pressure, atm
p_i	partial pressure of component i, atm
R	gas constant, 8.3143 J/(mol)(K), or other appropriate units
R_{ext}	external electrical resistance, Ω
R_{int}	internal electrical resistance, Ω
ΔS_o°	standard state entropy change, kJ/mol
T	temperature, in Kelvin unless otherwise stated
x_i	mole fraction of species i

Greek

α	transfer coefficient
η	overvoltage, V

Superscripts and subscripts

act	activation
CO_2	carbon dioxide
H_2	hydrogen
H_2O	water
O_2	oxygen
N_2	nitrogen
*	effective value

REFERENCES

1. R. M. Baumert, Master's Thesis, Queen's University, Kingston, ON, Canada (1993).
2. J. C. Amphlett, R. M. Baumert, T. J. Harris, R. F. Mann, B. A. Peppley, and P. R. Roberge, *This Journal*, **142**, 1 (1995).
3. D. S. Watkins, K. Dircks, D. Epp, and C. De La Franier, Paper presented at 4th Annual Battery Conference, Long Beach, CA, 1989.
4. D. S. Watkins, K. Dircks, D. Epp, and J. Blair, Paper presented at 5th Annual Battery Conference, Long Beach, CA, 1990.
5. J. C. Amphlett, M. Farahani, R. F. Mann, B. A. Peppley, and P. R. Roberge, in *Proceedings of 26th Intersociety Energy Conversion Conference*, pp. 624-630, IECEC (1991).
6. H. Ide, T. Yoshida, H. Ueda, and N. Horiuchi, in *Proceedings of 24th Intersociety Energy Conversion Conference*, pp. 1517-1522, IECEC (1989).
7. A. Cisar, in *Proceedings of 26th Intersociety Energy Conversion Conference*, pp. 611-616, IECEC (1991).
8. *Handbook of Fuel Cell Technology*, C. Berger, Editor, Prentice Hall, Englewood Cliffs, NJ (1968).
9. S. Srinivasan, O. A. Velev, A. Parthasarthy, D. J. Manko, and A. J. Appleby, *NASA Conf. Publ.*, No. 3195, pp. 101-122.
10. M. W. Verbrugge and D. M. Bernardi, *AIChE J.*, **37**, 1151 (1991).
11. T. E. Springer, T. A. Zawodzinski, and S. Gottesfeld, *This Journal*, **138**, 2334 (1991).
12. S. J. Ridge, R. E. White, Y. Tsou, R. N. Beaver, and G. A. Eisman, *ibid.*, **136**, 1902 (1989).